PHYSICAL REVIEW B **75**, 201201(R) (2007)

Dopant segregation and giant magnetoresistance in manganese-doped germanium

A. P. Li,[1,2] C. Zeng,[3] K. van Benthem,[1,2] M. F. Chisholm,[2] J. Shen,[1,2] S. V. S. Nageswara Rao,[4,5] S. K. Dixit,[4] L. C. Feldman,[2,4,5] A. G. Petukhov,[6] M. Foygel,[6] and H. H. Weitering[2,3]

[1]*Center for Nanophase Materials Sciences, Oak Ridge National Laboratory, Oak Ridge, Tennessee 37831, USA*

[2]*Materials Science and Technology Division, Oak Ridge National Laboratory, Oak Ridge, Tennessee 37831, USA*

[3]*Department of Physics and Astronomy, The University of Tennessee, Knoxville, Tennessee 37996, USA*

[4]*Interdisciplinary Program in Materials Science, Vanderbilt University, Nashville, Tennessee 37235, USA*

[5]*Department of Physics and Astronomy, Vanderbilt University, Nashville, Tennessee 37235, USA*

[6]*Physics Department, South Dakota School of Mines and Technology, Rapid City, South Dakota 57701, USA*

(Received 18 April 2007; published 10 May 2007)

Dopant segregation in a Mn_xGe_{1-x} dilute magnetic semiconductor leads to a remarkable self-assembly of Mn-rich nanocolumns, embedded in a fully compensated Ge matrix. Samples grown at 80 °C display a giant positive magnetoresistance that correlates directly with the distribution of magnetic impurities. Annealing at 200 °C increases Mn substitution in the host matrix above the threshold for the insulator-metal transition, while maintaining the columnar morphology, and results in global ferromagnetism with conventional negative magnetoresistance. The qualitative features of magnetism and transport in this nanophase material are thus extremely sensitive to the precise location and distribution of the magnetic dopants.

DOI: 10.1103/PhysRevB.75.201201 PACS number(s): 75.50.Pp, 61.72.−y, 73.50.Jt, 75.47.De

Chemical doping or the intentional introduction of impurities into a host material is fundamental to controlling its functional properties and is often a trigger for the emergence of novel physical phenomena. High-temperature superconductivity in doped Mott insulators,[1] colossal magnetoresistance in manganites,[2] and high temperature ferromagnetism in dilute magnetic semiconductors (DMSs),[3] have all been discovered via controlled doping experiments. Understanding the underlying physical principles of these emergent phenomena has become one of the key challenges in condensed matter physics just as their built-in functionalities foretell new technologies.

Heavily doped ferromagnetic DMSs are of great interest because of their potential applications in semiconductor spintronics. Recent studies on DMSs have shown that the growth conditions and sample treatment, such as postannealing, play a critical role in determining the distribution of magnetic dopants and their collective magnetic response.[4] Although ferromagnetism in "conventional" DMS materials such as $Mn_xGa_{1-x}As$ and Mn_xGe_{1-x} ($x \approx 0.05$) seems to be mediated by p-type charge carriers,[5,6] the lattice location and distribution of the individual dopant atoms critically affect their charge state and magnetic coupling, particularly in the insulating DMS.[7–14] The importance of inhomogeneities in heavily doped, conventional semiconductor systems is generally recognized, and usually considered undesirable. The equivalent assertion still requires experimental testing for new systems of current interest such as DMS materials. In fact, progress in this field would be greatly facilitated by quantitative analyses of the nature and consequences of disorder and inhomogeneity.

In this paper, we (1) determine the dopant distribution in Mn_xGe_{1-x} quantitatively; (2) tune the substitutional dopant fraction by a postannealing process; and (3) discover an intricate connection between the dopant location and magnetotransport properties from experiment and theory. The Mn dopants exhibit a remarkable tendency toward self-organization into arrays of Mn-rich nanocolumns. In the as-grown material, these columns are embedded in a crystalline Ge matrix in which substitutional acceptors and interstitial donors are almost perfectly compensated. This insulating DMS exhibits a giant positive magnetoresistance (MR). The dopant atoms are redistributed upon postannealing, resulting in global ferromagnetism with small negative MR. A phenomenological transport theory is developed, which quantitatively accounts for the observed changes in the MR. The surprising and extraordinary sensitivity to the site location and spatial distribution of the Mn can be traced to the competing effects of magnetic anisotropy, dipolar coupling, and carrier-mediated exchange between the nanocolumns.

Mn_xGe_{1-x} epitaxial films (700 Å in thickness) were grown on Ge(100) substrates with molecular beam epitaxy. The growth temperature was limited to 80 °C, so as to avoid formation of ferromagnetic intermetallic phases such as $Mn_{11}Ge_8$ and Mn_5Ge_3. Details of the sample preparation and magnetic properties of as-grown films are described in Ref. 9. Samples were examined using both conventional bright-field imaging in a transmission electron microscope (TEM) and high-resolution Z-contrast imaging in a scanning transmission electron microscope (STEM). A cross-sectional bright-field TEM image of an as-grown $Mn_{0.05}Ge_{0.95}$ film is shown in Fig. 1(a). The film contains columnar features that extend from the DMS/buffer layer interface to the film surface. Upon closer inspection, the columnar features appear to be strings of vertically elongated nanoclusters. Figure 1(b) shows the same material in plan view. The spatial distribution of these columns is not random; instead, the columns have a fairly uniform size distribution with an average column diameter of 2 nm and a pair correlation length of 7 nm. Annular dark-field STEM observations of the columnar structures with varying inner detector angles [see Figs. 1(c) and 1(d)] show that the nanocolumns are highly strained and contain some degree of disorder. In the following, we will call the structure "disordered." The spatial profile of the Mn,

 ©2007 The American Physical Society

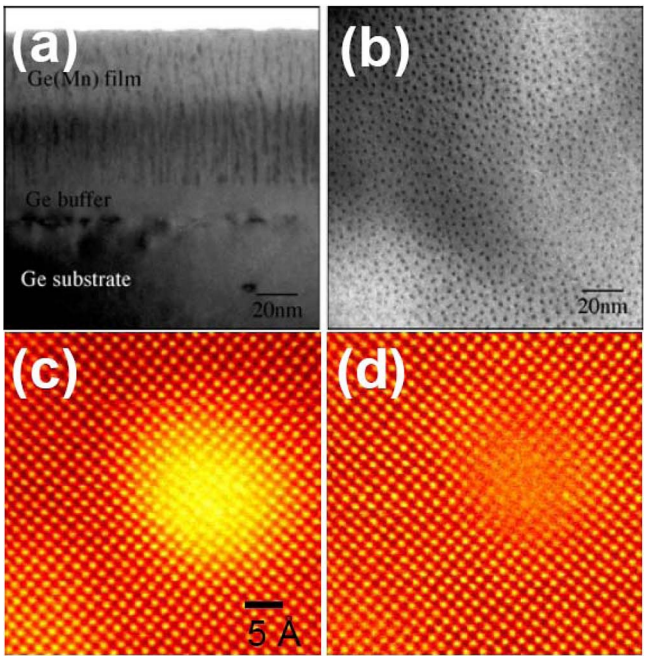

FIG. 1. (Color online). Nanoscale phase separation in as-grown $Mn_{0.05}Ge_{0.95}$. (a) Cross-sectional TEM image; (b) plan-view TEM image; (c) STEM image highlighting strain contrast (~35 mrad inner detector angle); and (d) STEM image highlighting Z-contrast (~60 mrad inner detector angle).

obtained using *L*-shell electron energy loss spectroscopy (EELS), indicates that Mn is located primarily inside the nanocolumns, with little Mn in between the nanocolumns. Postannealing to 200 °C in vacuum for 2 h did not produce noticeable changes in morphology and diffraction patterns; Mn_5Ge_3 crystallites nucleate above 250 °C.

The lattice location of the dopants and global stoichiometry of the as-grown and postannealed films were studied with channeling Rutherford backscattering spectrometry (RBS).[15] Figure 2 shows the channeling angular scans measured about ⟨100⟩ directions of the as-grown and the postannealed $Mn_{0.1}Ge_{0.9}$ samples. The Ge minimum yields (χ_{min}), determined from the near-surface region of both samples, are higher than those of high-quality Ge crystals. This indicates

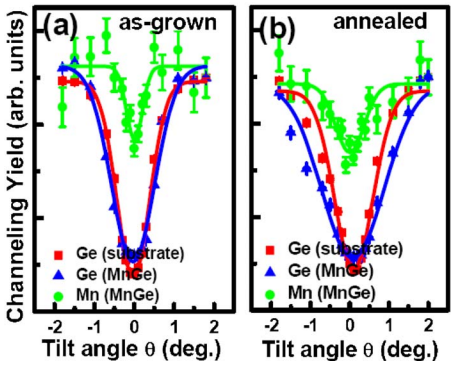

FIG. 2. (Color online). Channeling RBS angular scans about the ⟨100⟩ axes for as-grown (a) and postannealed (b) $Mn_{0.1}Ge_{0.9}$ samples.

TABLE I. Mn dopant distribution in $Mn_{0.1}Ge_{0.9}$ obtained from ion channeling.

Sample	Stoichiometry of nanocolumns	Nonrandom fraction (f_{nr}) ⟨100⟩	Nonrandom fraction (f_{nr}) ⟨110⟩
As grown	$Mn_{0.17\pm0.03}Ge_{0.83\pm0.03}$	0.36±0.04	0.24±0.04
Postannealed	$Mn_{0.3\pm0.04}Ge_{0.7\pm0.04}$	0.42±0.04	0.50±0.04

some degree of noncrystallinity in the film, which is consistent with the TEM observations. The χ_{min} values for Mn are clearly higher than those of Ge, which indicates that the Mn atoms are mostly nonsubstitutional. Upon annealing at 200 °C, χ_{min}^{Mn} decreases dramatically along the ⟨100⟩ direction as compared to the as-grown sample. Evidently, some interstitial Mn (Mn_i) have been converted to substitutional Mn (Mn_s) during the annealing process.

The diamond lattice contains three likely locations for Mn_i, two tetrahedral sites and one hexagonal, in which the atoms are exposed in the ⟨110⟩ axial channel, but shadowed by the host Ge atoms when viewed along the ⟨100⟩ channel.[16,17] Atoms in the disordered columns are exposed in all channeling directions. For the as-grown sample, the nonrandom fraction of Mn ($f_{nr}=[1-\chi_{min}^{Mn}]/[1-\chi_{min}^{Ge}]$) is 0.36±0.04 along the ⟨100⟩ direction and 0.24±0.04 along the ⟨110⟩ direction (displayed in Table I). Accordingly, we infer that ~24% of Mn atoms is Mn_s, 12% is Mn_i, and 64% is randomly distributed and presumably incorporated in the nanocolumns. Because Mn_i is a double donor and Mn_s is an acceptor,[18] the Ge matrix must be almost perfectly compensated, consistent with the observation of a very low "effective carrier density" in Hall effect measurements.[6,9,10] Upon annealing at 200 °C, $f_{nr}^{\langle 100\rangle}$ no longer differs significantly from $f_{nr}^{\langle 110\rangle}$ (Table I), indicating that there are (almost) no left-over Mn_i. Upon postannealing, the areal density of Ge in the columns decreases from 13.7×10^{16} to 6.69×10^{16} atoms/cm^2 while that of Mn remains constant ($\sim2.9\times10^{16}$ atoms/cm^2). These areal density counts suggest an apparent stoichiometry of $Mn_{0.17}Ge_{0.83}$ and $Mn_{0.3}Ge_{0.7}$ of the nanocolumns in as-grown and postannealed materials, respectively.

Figure 3(a) shows the remanent magnetization of the as-grown and postannealed $Mn_{0.05}Ge_{0.95}$ samples as a function of temperature. Whereas the magnetic remanence of the as-grown samples vanishes near ~12 K, postannealed samples exhibit remanence up to about 125 K. Furthermore, the saturation magnetization increases from $1.0\mu_B$ to $1.5\mu_B$ per Mn atom upon postannealing (inset). Postannealing thus leads to a very substantial improvement of the magnetic properties. Figure 3(b) shows the ac magnetic susceptibility of both samples. The ac response of the as-grown sample peaks near 12 K, consistent with the onset of remanence.[9,10] On the other hand, the ac response of the postannealed sample exhibits a pronounced maximum at 125 K and a shoulder near 60 K. These features shift to higher and lower temperatures, respectively, upon applying a dc magnetic field. Similar behavior in other materials has been attributed to the formation

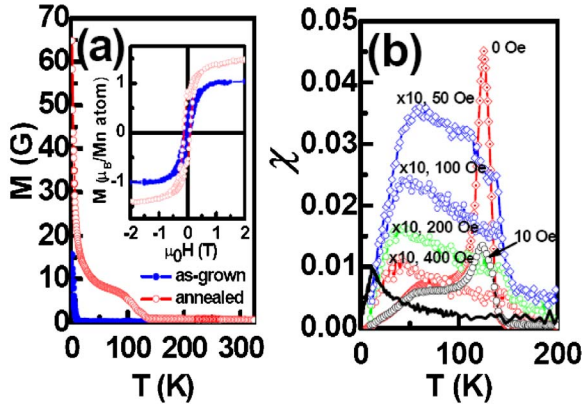

FIG. 3. (Color online). (a) Remanent magnetization of $Mn_{0.05}Ge_{0.95}$ as a function of temperature, before and after postannealing. The inset shows the dc magnetization at 5 K with the field perpendicular to the sample surface. (b) Temperature-dependent ac susceptibility of postannealed $Mn_{0.05}Ge_{0.95}$ measured in various dc fields and as-grown $Mn_{0.05}Ge_{0.95}$ (solid line) in zero dc field. H_{ac} =5 Oe, f=24 Hz.

of a spin glass[19] or clustered spin system,[20] which in the present case is naturally attributed to the presence of Mn-rich nanocolumns.

Figure 4 shows MR isotherms of the as-grown (a) and postannealed (b) $Mn_{0.05}Ge_{0.95}$ samples. The contrast is quite dramatic. As-grown samples reveal a *giant positive MR* between 50 and 200 K, which is roughly proportional to the square of the magnetization curve (MR measurements were not feasible below 50 K due to the highly resistive nature of the as-grown film). On the other hand, postannealing dramatically reduces the MR, revealing both positive and negative contributions, with the negative contribution dominating at high field. The latter is typical for spin disorder scattering in metallic DMS.[21] Indeed, postannealing converted the Mn_i into Mn_s, which we estimate increases the fraction of uncompensated acceptors to about 1.8% or 8.0×10^{20} cm^{-3}. This concentration is well above the threshold for the insulator-metal phase transition that apparently takes place during the postannealing process. In the following, we will show that a giant positive MR of the as-grown samples *must be* due

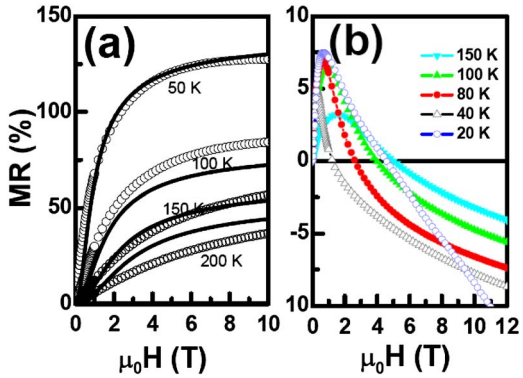

FIG. 4. (Color online). (a) Giant MR of as-grown $Mn_{0.05}Ge_{0.95}$ at different temperatures. The solid lines represent theoretical fits, according to Eq. (1). (b) MR of postannealed $Mn_{0.05}Ge_{0.95}$.

to magnetic anisotropy and antiferromagnetic (AFM) interactions, which in turn is attributed to the columnar morphology.

The zero-field resistivity of the as-grown sample is almost temperature independent between 50 and 200 K.[10] Thus uncompensated Mn acceptors are likely ionized and the MR is directly correlated with the hole mobility, which in turn is limited by the magnetic disorder associated with the randomly distributed Mn nanoclusters with spin J and volume concentration N. Following Refs. 22 and 23 one can find scattering probability and calculate the mobilities of the carriers in the spin-split subbands.[22] An estimation of the MR of the nondegenerate magnetic semiconductor in this temperature region is then

$$\frac{\rho(H)-\rho(0)}{\rho(0)} \approx \frac{k_B T[\chi_{\parallel}(H)+2\gamma\chi_{\perp}(H)]+(g\mu_B)^2 N\langle J_z\rangle^2}{k_B T(1+2\gamma)\chi_{\parallel}(0)} - 1. \quad (1)$$

Here g is the Landé factor of the ionic spins, and μ_B is the Bohr magneton. Also, $\langle J_z\rangle = JB_J(J\alpha) = M(H)/g\mu_B N$ is the thermodynamically averaged projection of the nanocluster spin onto the direction of magnetic field, with $M(H)$ being the magnetization, $B_J(J\alpha)$ the Brillouin function, and $\alpha \approx g\mu_B H/k_B T$ in the paramagnetic phase. The longitudinal and transverse magnetic susceptibilities are $\chi_{\parallel}=\partial M/\partial H$ and $\chi_{\perp}=M/H$, respectively. The term in the brackets in the numerator of Eq. (1) describes scattering by thermal spin fluctuations, while the last term represents scattering by spatial fluctuations of the local concentrations of magnetic nanoclusters. In deriving Eq. (1) we introduced a phenomenological anisotropy factor $\gamma<1$, which was motivated by the experimental observations. The terms proportional to $\chi(H)$ decrease with the magnetic field H: the mobility increases due to the suppression of thermal spin fluctuations giving rise to negative MR. On the other hand, scattering by spatial fluctuations of the magnetic nanoclusters increases with H because local fluctuations in the Mn-induced band splitting increase with H.[23] This decreases the mobility and produces positive MR. In the absence of magnetic anisotropy ($\gamma=1$), these competing spin-scattering mechanisms normally lead to a small but negative MR.[24]

Above 20 K, the magnetic data of as-grown Mn_xGe_{1-x} collapse onto the Langevin function $L(y)$,[9] which is a signature of a superparamagnetic system ($J\gg1$). For such a system, $B_J(y)\rightarrow L(y)$, with $y=Jg\mu_B H/k_B T$ and, according to Eq. (1) $\Delta\rho/\rho(0)=0$ if $\gamma=1$. Smaller values of J always produce a small negative MR. In fact, the large positive MR of the as-grown samples can only be explained by including AFM interactions, even if $\gamma=1$. Indeed, by replacing the argument of $L(y)$ with $y=Jg\mu_B H/k_B(T+T_{AF})$ where $T_{AF}>0$ is the AFM temperature, we obtain a positive MR: $\Delta\rho/\rho(0) = L^2(y)T_{AF}/T$. Magnetic anisotropy($\gamma<1$) further enhances the positive MR because it suppresses transverse spin fluctuations. Figure 4(a) shows a fit to four different MR isotherms, using Eq. (1) with $T_{AF}=15$ K and $\gamma=0.35$. The quality of the fit is quite good, considering the fact that it only uses two adjustable parameters for different isotherms covering a very wide temperature range. The agreement can be

improved if one takes into account the magnetic field dependence of the carrier concentration with the detailed complex structure of the hole bands.

The following picture thus emerges. The nanocolumns are locally ferromagnetic. The magnetic dipolar coupling between the columns competes with the carrier mediated exchange interactions. Due to the near perfect compensation of the host matrix, the carrier mediated exchange is very weak. The dominant dipolar coupling most likely favors AFM alignment between the columns but the magnetic remanence remains finite near 0 K due to the geometrical magnetic frustration in the AFM array of nanocolums.[14] Postannealing increases the Mn_s fraction and net hole concentration in the host matrix, which is qualitatively consistent with a reduction of the sheet resistance by a factor of 4 and the increase of the carrier concentration by a factor of 20 from the normal Hall coefficient (not shown). This dipolar coupling is then easily overwhelmed by carrier mediated exchange. Consequently, the positive MR is strongly suppressed, leading to a weak negative MR, characteristic of carrier scattering by thermodynamic spin fluctuations.[21]

In conclusion, quantitative analysis of the dopant distribution in as-grown and postannealed Mn_xGe_{1-x} DMS reveals an intriguing self-organization of dopants at the nanoscale. The magnetization and MR data clearly correlate with these findings and highlight the critical aspects of magnetic shape anisotropy, dipolar interactions, and carrier mediated exchange. This study furthermore indicates the general need of including realistic doping distributions in theoretical studies of these complex materials.

Recently, we became aware of a publication by Jamet *et al.*,[14] who observed similar nanocolumns, although the composition, structure, and spatial distribution of the nanocolumns are slightly different. In contrast to our work, Jamet *et al.* observe a ferromagnetic $T_C > 400$ K and an unexplained giant orbital MR that appears to be totally unrelated to the magnetization, which reinforces the notion that the MR is extremely sensitive to the dopant distribution.

This work was supported in part by the Center for Nanophase Materials Sciences at Oak Ridge National Laboratory (ORNL), which is sponsored by the DOE Division of Scientific User Facilities (A.P.L. and J.S.). The authors furthermore acknowledge support from the DOE Division of Materials Sciences and Engineering under Contract No. DE-AC05-00OR22725 (H.H.W., K.v.B., and M.F.C.), and from NSF Contract No. DMR 0606485 (C.Z. and H.H.W.), and ONR Contract No. N00014-06-1-0616 (A.G.P. and M.F.). K.vB. was appointed through the ORNL Postdoctoral Research Program, which is administered jointly by ORNL and ORISE. ORNL is managed and operated by UT-Battelle, LLC.

[1] A. Damascelli, Z. Hussain, and Z.-X. Shen, Rev. Mod. Phys. **75**, 473 (2003).

[2] E. Dagotto, Science **309**, 257 (2005).

[3] H. Ohno, H. Munekata, T. Penney, S. von Molnár, and L. L. Chang, Phys. Rev. Lett. **68**, 2664 (1992).

[4] K. W. Edmonds, P. Bogusawski, K. Y. Wang, R. P. Campion, S. N. Novikov, N. R. S. Farley, B. L. Gallagher, C. T. Foxon, M. Sawicki, T. Dietl, M. Buongiorno Nardelli, and J. Bernholc, Phys. Rev. Lett. **92**, 037201 (2004).

[5] T. Dietl, H. Ohno, F. Matsukura, J. Cibert, and D. Ferrand, Science **287**, 1019 (2000).

[6] Y. D. Park, A. T. Hanbicki, S. C. Erwin, C. S. Hellberg, J. M. Sullivan, J. E. Mattson, T. F. Ambrose, A. Wilson, G. Spanos, and B. T. Jonker, Science **295**, 651 (2002).

[7] J.-S. Kang, G. Kim, S. C. Wi, S. S. Lee, S. Choi, Sunglae Cho, S. W. Han, K. H. Kim, H. J. Song, H. J. Shin, A. Sekiyama, S. Kasai, S. Suga, and B. I. Min, Phys. Rev. Lett. **94**, 147202 (2005).

[8] S. Cho, S. Choi, S. C. Hong, Y. Kim, J. B. Ketterson, B.-J. Kim, Y. C. Kim, and J.-H. Jung, Phys. Rev. B **66**, 033303 (2002).

[9] A. P. Li, J. F. Wendelken, J. Shen, L. C. Feldman, J. R. Thompson, and H. H. Weitering, Phys. Rev. B **72**, 195205 (2005).

[10] A. P. Li, J. Shen, J. R. Thompson, and H. H. Weitering, Appl. Phys. Lett. **86**, 152507 (2005).

[11] C. Jaeger, C. Bihler, T. Vallaitis, S. T. B. Goennenwein, M. Opel, R. Gross, and M. S. Brandt, Phys. Rev. B **74**, 045330 (2006).

[12] C. Bihler, C. Jaeher, T. Vallaitis, M. Gjukic, M. S. Brandt, E. Pippel, J. Woltersdorf, and U. Goesele, Appl. Phys. Lett. **88**, 112506 (2006).

[13] M. Passacantando, L. Ottaviano, F. D'Orazio, F. Lucari, M. De Biase, G. Impellizzeri, and F. Priolo, Phys. Rev. B **73**, 195207 (2006).

[14] M. Jamet, A. Barski, T. Devillers, V. Poydenot, R. Dujardin, P. Bayle-Guillemaud, J. Rothman, E. Bellet-Amalric, A. Marty, J. Cibert, R. Mattana, and S. Tatarenko, Nat. Mater. **5**, 653 (2006).

[15] For the full channeling angular scans, we used a $Mn_{0.1}Ge_{0.9}$ sample, which produces stronger signals. The 10% sample was found by TEM to exhibit the same columnar morphology seen in the 5% Mn sample.

[16] K. M. Yu, W. Walukiewicz, T. Wojtowicz, I. Kuryliszyn, X. Liu, Y. Sasaki, and J. K. Furdyna, Phys. Rev. B **65**, 201303 (2002).

[17] J. Blinowski and P. Kacman, Phys. Rev. B **67**, 121204(R) (2003).

[18] S. C. Erwin and A. G. Petukhov, Phys. Rev. Lett. **89**, 227201 (2002).

[19] D. Hueser, L. H. Wenger, A. J. van Duyneveldt, and J. A. Mydosh, Phys. Rev. B **27**, 3100 (1983).

[20] I. G. Deac, J. F. Mitchell, and P. Schiffer, Phys. Rev. B **63**, 172408 (2001).

[21] F. Matsukura, H. Ohno, A. Shen, and Y. Sugawara, Phys. Rev. B **57**, R2037 (1998).

[22] P. G. De Gennes and J. Friedel, J. Phys. Chem. Solids **4**, 71 (1958).

[23] C. Haas, Phys. Rev. **168**, 531 (1968).

[24] D. Schmidt, A. G. Petukhov, M. Foygel, J. P. Ibbetson, and S. J. Allen, Phys. Rev. Lett. **82**, 823 (1999); A. G. Petukhov and M. Foygel, Phys. Rev. B **62**, 520 (2000). Polaronic transport models considered in these papers can also account for positive MR but we could not obtain reasonable data fits in the temperature range 50–200 K using these models.